Polímeros
ISSN 1678-5169 (Online)

https://doi.org/10.1590/0104-1428.20240075

ORIGINAL ARTICLES

Recovery of the post-industrial recycled ABS thermomechanical properties by adding graphene oxide

Lucas Pacanaro de Lima[1,2], André Petraconi[1,2], Natália Ferreira Braga[1,2], Lidiane Cristina Costa[3], Ricardo Jorge Espanhol Andrade[1,2] and Guilhermino José Macêdo Fechine[1,2*]

[1]Escola de Engenharia, Universidade Presbiteriana Mackenzie, São Paulo, SP, Brasil
[2]Instituto Mackenzie de Pesquisa em Grafeno e Nanotecnologias - MackGraphe, Universidade Presbiteriana Mackenzie, São Paulo, SP, Brasil
[3]Departamento de Engenharia de Materiais, Universidade Federal de São Carlos – UFSCar, São Carlos, SP, Brasil
**guilherminojmf@mackenzie.br*

Abstract

The post-industrial recycled ABS (ABSpost) was used to produce a new material based on graphene oxide (GO), aimed at high-quality products again, as households and electronic applications. The GO was prepared from the oxidation of graphite, and the influence of the different amounts of filler on the mechanical, rheological, and thermal properties of ABSpost was investigated. The X-ray microtomography showed a uniform dispersion of GO fillers in the ABSpost matrix in small amounts (0.05 and 0.1 wt%), improving some properties, such as elongation at break, toughness, and impact strength. The thermal conductivity of the ABSpost also increases by 30% with the addition of only 0.1 wt% of GO. Adding a small amount of GO in a recycled ABS is a strategy to deal with the current problem of electronic housing waste and use this material to minimize its environmental impact.

Keywords: *post-consumer ABS, graphene oxide, polymer nanocomposites.*

How to cite: Lima, L. P., Petraconi, A., Braga, N. F., Costa, L. C., Andrade, R. J. E., & Fechine, G. J. M. (2025). Recovery of the post-industrial recycled ABS thermomechanical properties by adding graphene oxide. *Polímeros: Ciência e Tecnologia*, *35*(2), e20250013. https://doi.org/10.1590/0104-1428.20240075

1. Introduction

The concern about environmental impact related to the wrong waste and disposal of polymer materials leads to a necessity of reusing these materials until, ultimately, the life cycle considering the circular economy: production, use, recycling, and reuse[1]. In the last decade, electronic product consumption increased, and consequently, a similar growth in waste from electrical and electronic equipment (WEEE) was noted[2]. Acrylonitrile butadiene styrene (ABS) is an engineering thermoplastic mainly used in electrical and electronic equipment, such as cell phones, laptops, computers, TVs, and so on, due to its characteristics, such as mechanical strength, toughness and rigidity, and relatively low-cost processing[3]. One problem is that this material takes time to degrade after its use, causing its reuse and recycling as a tool to be sought. In addition, chemicals hazardous to the environment are produced when these materials are incorrectly disposed of in nature, making their reuse a vital necessity[4].

Reintroducing a recycled polymer into the market requires some modification once the recycling process can alter the overall properties of those materials. Several strategies have been used for ABS recycling to reduce their environmental impact, for example, creating polymer blends[3-6], aiming to reuse this polymer without much decrease in its properties compared to virgin ABS. Brennan et al.[5] studied the mechanical properties of ABS and high-impact polystyrene (HIPS) blends from computer equipment waste. The presence of 10% ABS in HIPS or 10% of HIPS in ABS had a favorable effect on the strains to failure, indicating a recovery of mechanical properties, such as ductility, that is commonly lost in each independent polymer during the recycling process due to degradation. In another study, Saxena and Maiti[4] prepared a blend of ABS from electronic waste with low-density polyethylene (LDPE) with maleic anhydride (MA) as a compatibilizing agent via reactive extrusion in a twin-screw extruder. The blends presented enhancement in mechanical properties, for example, an increase of up to 246% in Young´s modulus compared to the neat HDPE due to MA, which created a crosslink structure in the system. Scaffaro et al.[3] made a polymer blend mixing post-consumed ABS with virgin ABS resin in different proportions and studied their properties after different recycling cycles. The rheological measurements showed no change in the viscosity of the ABS blends up to two recycling cycle steps compared to virgin ABS.

Besides the use of polymer blends, another approach is using nanofillers as reinforcement for recycled ABS. As reported in the study made by Mao et al.[7], the authors verified the effect of adding montmorillonite and nitrile rubber in recycled ABS: results showed an improvement in the mechanical properties (impact strength, tensile strength, and tensile modulus) of recycled ABS when adding 1 phr of montmorillonite in re-ABS/NBR (90/10).

Here, the study aims to develop a strategy to use Post-Industrial Recycled ABS as a raw material for producing plastic parts. This strategy is by inserting a nanometric filler, graphene oxide (GO), in the polymer matrix. Graphene-reinforced polymer nanocomposites have attracted attention due to their excellent properties and multifunctionalities, which are widely applied in many fields[8,9]. Some studies have shown that inserting graphene and its derivatives in an ABS matrix increases the mechanical and thermal properties and rheological measurements[10–13]. Compared to other fillers, graphene stands out due to its large specific area and high aspect ratio, and using only small amounts of this filler, it is possible to enhance the electrical, mechanical, and barrier characteristics of the polymer[8,14]. Moreover, the functional groups present on the surface of the GO, such as epoxy, hydroxyl, carbonyl, and carboxyl groups, can improve the interaction within the matrix, enhancing the dispersion[15,16].

In this context, this study aimed to evaluate the effect of adding different amounts of GO on post-industrial recycled ABS (ABSpost) properties to recover some specific properties that allow it to be used again in non-commodity items. Adding GO to ABS_{post} attempts to overcome the barriers to recycling electronic equipment and reusing polymers to minimize their environmental impact.

2. Materials and Methods

The Post-Industrial Recycled ABS (ABS_{post}) was obtained from AKG Reciclagem de Plásticos Company in Brazil. Sigma Aldrich supplied the powdered graphite (99% purity). Sulfuric acid, potassium permanganate, hydroxyl peroxide, hydrochloric acid, and ethanol were used in GO synthesis.

2.1 Synthesis of graphene oxide (GO)

The GO was synthesized by Hummer's method modified, as described by Pinto et al.[17] In the first step, the oxidation of graphite prepared the graphite oxide (GrO): slowly added 60 ml of sulfuric acid in 1g of graphite in an ice bath and stirred for 15 min, followed by the addition of 100 ml of a solution of $KMnO_4$ (35 mg/ml) with the aid of a peristaltic pump using a flow rate of 6.8 ml/min. After adding the $KMnO_4$ solution, the system was stirred in ice for 5 minutes. The ice bath was removed, and the system was stirred for 2 hours. Then, the system was diluted in 100 mL of distilled water, followed by a hydroxyl peroxide 30% addition until bubble formation ceased. After 24h rest, the GrO was precipitated and washed with 500 ml of water, 250 mL of 10% hydrochloric acid, 250 ml of ethanol, and 200 ml of water. Then, the GrO was filtered and dried in a vacuum oven for 12h at 60°C.

In the second step, the GrO was dispersed in distilled water at a 1 mg/ml concentration to exfoliate using an ultrasonic bath (Elma—P30H) for 2 hours, obtaining the GO suspension.

2.2 Filler characterization

Thermo-gravimetric analysis (TGA) for the pristine graphite and GrO was made using a TA instrument (DSC/TGA Q600) at a nitrogen atmosphere between 30 and 1000°C at a rate of 10°C/min using an alumina crucible. The graphite and GrO were characterized by X-ray diffraction (XRD) in a Rigaku MiniFlex II with incident radiation of 1.42 Angstroms of wavelength number. The scanning angle was 3° to 60° at a 2°/min rate. The Raman Spectroscopy of graphite and GrO was made in a Witec model Alpha 300R operating at a 532 nm wavelength incident laser. The GO was characterized using atomic force microscopy (AFM) in an Icon Dimension (Bruker) equipped with RTESPA. The GO suspension was dropped in a mica substrate to be analyzed.

2.3 Nanocomposites preparation

The ABS_{post} was grounded using a milling knife (SL 31—Solab Científica) to increase the surficial area of the polymer grains. The polymer powder was mixed with the GO suspension to produce ABSpost/GO systems with different concentrations of filler: 0.05 wt.%, 0.1 wt. %, and 0.3 wt. %. The solid-solid deposition (SSD) technique18 was used, in which the components were mixed and heated until complete solvent evaporation, obtaining polymer grains covered with GO particles.

The ABS_{post} and the nanocomposites were then mixed by melting using a twin-screw extruder model Process 11 of ThermoScientific (L/D = 40). The screw speed used was 150 rpm, and a feeder of 4g/min. The temperature in each extruder section was 180, 190, 200, 210, 220, 220, 215, and 210°C from the first zone to die. The extrudate filament was cooled in water and cut up to obtain pellets.

Specimens for the tensile and impact tests of the ABSpost and the nanocomposites were molded using an injection molding machine, the Haake Minijet Pro from Thermo Scientific. The cylinder and mold temperatures were 230°C and 90°C, respectively. The injection pressure was 250 bar for 25 seconds, and the post pressure was 120 bar for 10 seconds.

2.4 Nanocomposites characterization

The mechanical properties of the nanocomposites were analyzed using a Zwick/Roell Z100 according to ASTM D638-14 at room temperature, 5 mm/min speed, and load cell 10 kN. The parameters, such as Young´s modulus, tensile strength, tensile at break, elongation at break, and toughness (area below the stress x strain curve), were obtained.

The impact resistance test was performed according to Izod ISO 180 using a Tinius Olsen model IT 504. Before the test, the specimens were notched using a Tinius Olsen (model 899).

The fracture surface morphology of the notched impact specimens was analyzed by Scanning electron microscopy (SEM) using a Hitachi TM 3000, with an accelerating voltage of 15 kV. The specimens were covered with a thin

layer of gold using a Sputter Coater Bal-tec SCD 050, 40 mA for 30 seconds.

Dynamic Mechanical Analysis (DMA) was performed using PerkinElmer 8000 from 25°C to 150°C under air at a temperature increase rate of 3 °C/min applying a 0.05% strain with 1 Hz frequency, using two points bending mode.

Rheological tests were obtained using a rheometer Anton Paar (MCR 702) equipped with 25 mm parallel plate geometry with a gap of 1 mm at a temperature of 220ºC in a compressed air environment. Steady-state rheological measurements were performed to analyze the viscosity in the function of the shear rate ranging from 0.01 s^{-1} to 100 s^{-1}. Dynamic tests were also executed to investigate the viscoelastic properties of the material. Time sweep (120 min) and angular frequency sweep measurements ranging from 0.01-100 rad/s were conducted within the linear viscoelastic regime (LVR).

The thermal conductivity of the nanocomposites was measured using Trident thermal conductivity equipment from C-Therm with MTPS (*modified transient plane source*). It was tested at four temperatures (25, 40, 60, and 80 °C).

X-ray microtomography (XR-MT) analyzed the dispersion and distribution of the fillers within the matrix. It was performed using a Rigaku Nano 3DX, an X-ray source with a 1200W power supply, Mo radiation, 17 keV, and a 10x lens.

3. Results and Discussion

3.1 Graphite and GrO characterization

TGA analyzed the thermal stability of the pristine graphite and GrO (Figure 1). The pristine graphite is thermal stable in the temperature range studied, presenting no loss mass (the percentage maintains close to 100%), indicating the material's high crystallinity and purity[18]. The insertion of functionalized groups on GrO changes the material's thermal stability. It was possible to observe two steps of mass loss: the first at ~100 °C, due to the water elimination present between the GrO layers, and the other significant mass loss (~26.15%) between 170°C and 320°C, which refers to the loss of oxygen-containing groups[19,20], confirming that the oxidation process occurred.

The diffractograms obtained for graphite and GrO are presented in Figure 2. It was possible to verify that the graphite presents a sharp peak at $2\theta = 26.5°$ related to the plane (002) and another small peak at 54 ° related to the (004) plane[20], confirming the high crystalline nature of graphite. There is a displacement of the atomic plane (002) for $2\theta = 11.12°$ after oxidation in GrO. Peak enlargement is also notable due to the introduction of functional groups into the layers[21]. Using Bragg's equation (Equation 1): $n\lambda = 2dsin\theta$, where n is an integer number, λ is the X-ray wavelength, d is the interlayer space and θ is the incident angle; the distance of the lattice planes is 0.33 nm for graphite and 0.77 nm for GrO implies that the carbon layers were expanded due to the oxygen groups insertion on basal plane and bords[20].

Figure 3 shows the Raman spectra for the graphite and GrO. The G band presented in graphite and GrO at ~ 1570 cm^{-1} is related to the sp^2 hybridization of carbonic structure. In the GrO spectra is visible a peak at ~1350 cm^{-1}, related to the D band, and it is associated with defects in the graphitic structure, such as the presence of vacancies and functional groups, which lead to a disruption of the hexagonal graphitic lattice, being another indication of the graphite oxidation[22]. Finally, the 2D band ~ 2690 cm^{-1} can be related to the number of graphene layers; when the G band is intense and the 2D band less intense, it is assumed that the number of layers is high[23,24]. The reason for this is that GrO is still unexfoliated material.

The ratio between the D and G band intensities (ID/IG) allowed the number of defects in the material's structure to be estimated. The ID/IG was 0.97, indicating a low level of structural defects and oxidation[23].

The AFM analysis of GO was carried out to verify its flake thickness and lateral size, generating frequency histograms of lateral size and height of the GO sheets, presented in Figures 4a and b, respectively. The GO majority sheets present a height between 4 and 10 nm and an equivalent lateral size between 300 and 600 nm. Through the AFM images in Figure 4c, it was possible to verify that the particle size is not homogeneous; it can be inferred that

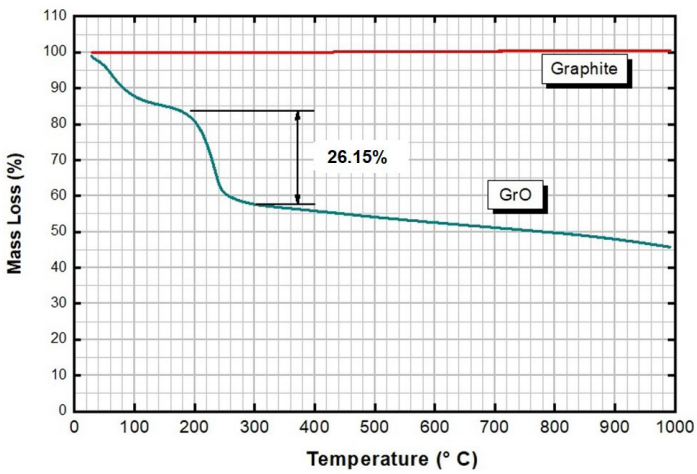

Figure 1. TGA of graphite and GrO.

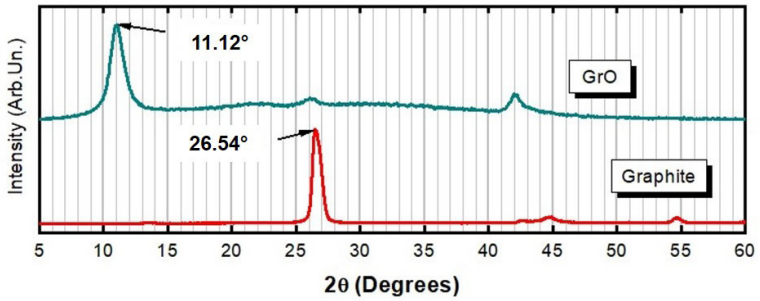

Figure 2. X-ray pattern of graphite and GrO.

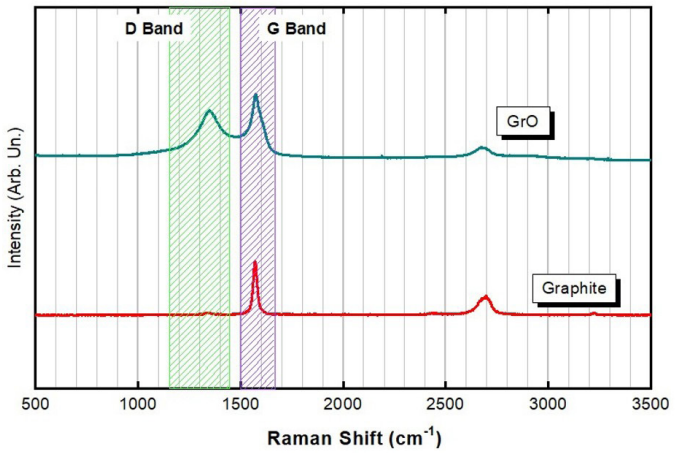

Figure 3. Raman spectra of graphite and GrO.

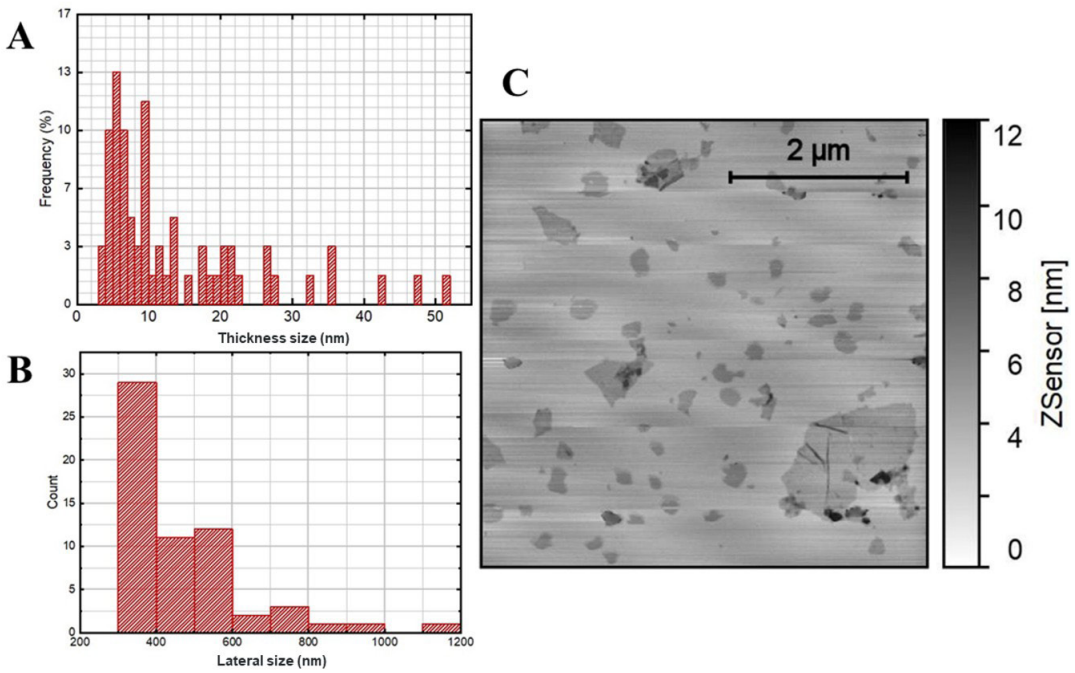

Figure 4. a) Frequency of the height, b) Count of lateral size, and c) AFM image of GO sheets.

the exfoliation process of GrO originated GO with different heights and lateral sizes. Graphene-like materials' size and thickness can largely influence the properties of the final nanocomposites: larger sheets, that is, larger lateral size, are suitable for improving the interaction with the polymer matrix, leading to better properties of the nanocomposite[25]. Kaczmarek et al.[26] "large" GO are those with lateral size exceeding 10 µm, "medium" flakes are between 3 and 10 µm, and "small" flakes have dimensions less than 3 µm. Small flakes present lower aspect ratio values, leading to difficulty transferring their properties to the matrix and, consequently, a slight improvement in nanocomposite properties.

3.2. ABS/GO nanocomposites characterization

3.2.1 X-Ray Microtomography

The homogeneous dispersion of GO in ABSpost is the most crucial criterion for successfully improving the properties of the nanocomposites. The XR-MT was carried out to investigate the filler dispersion and distribution within the matrix in 3D. Some characteristics of the particles were obtained, such as surface area and volume, which are listed in Table 1.

Table 1. Particle´s surface area and volume obtained by XR-MT.

Sample	Surface area (µm²)	Volume (µm³)
ABS_{post}/GO 0.05	4470045	6202577
ABS_{post}/GO 0.1	3638786	4042292
ABS_{post}/GO 0.3	2482784	4159074

Figure 5 shows the 3D images and the volume and surface area histogram of the ABS_{post}/GO nanocomposites. In the images, the red spots represent the filler, and as the filler volume/surface area decreases, the color becomes darker. The ABS_{post}/GO 0.05 presented the most homogeneous filler distribution pattern and the higher surface area and volume. The higher the surface area, the more efficient the interaction between filler and matrix is, which influences the property's transference from one to another. On the other hand, the nanocomposite with 0.3% GO has the smallest volume and surface area, weakening the material.

3.2.2 Mechanical properties

The stress-strain curves for the ABS_{post} and ABS_{post}/GO nanocomposites are presented in Figure 6. Through those curves, it was possible to obtain parameters such as Young's modulus (E), yield tensile strength (ys), tensile (σ_b) elongation (ε_b) at break, and toughness, which are summarized in Table 2.

The ABS_{post} shows a ductile material behavior with elastic deformation, yield point, and plastic deformation until the fracture. Usually, the mechanical properties of recycled and neat polymer materials are quite different. The neat ABS resin generally presents a tensile strength of around 40-48 MPa, Young´s modulus ~ 1.5-2.3 GPa, and strain at a break between 7 and 38%[27-30]. The processing of polymer and the recycling process can lead to losses in mechanical properties, mainly due to thermal degradation due to a decrease in molecular weight[31,32]. Here, it is possible to observe that the ABS_{post} presents values similar to Young´s modulus and maximum stress (yield point) compared to a neat ABS. Therefore, the strain at break data

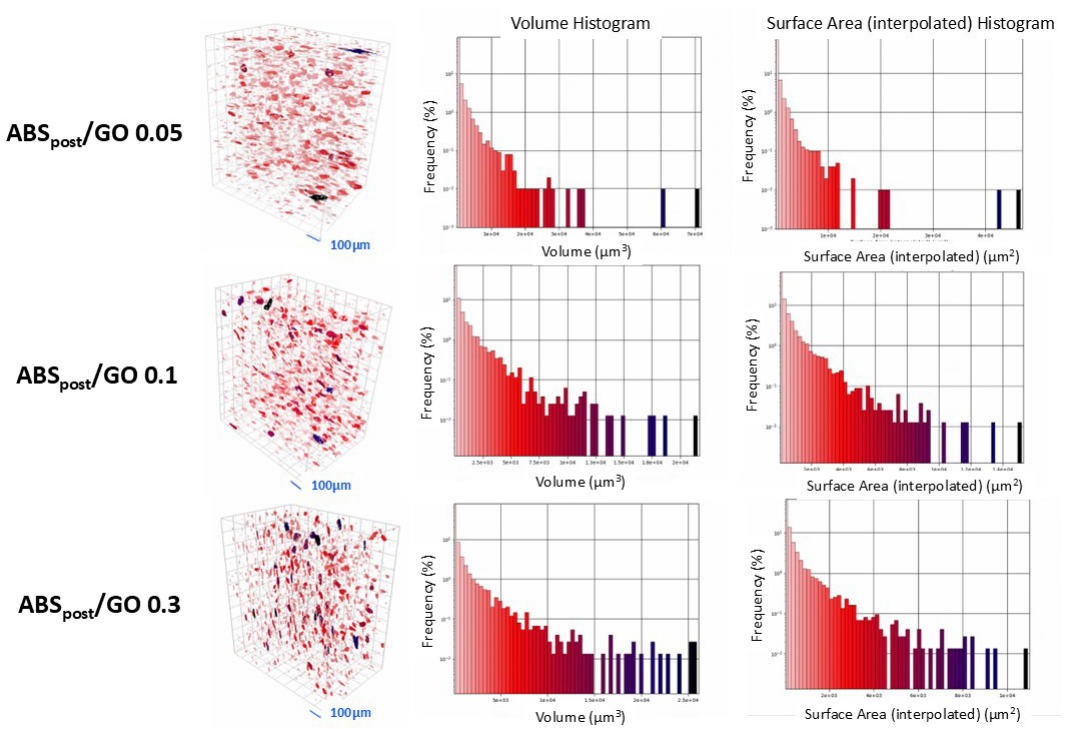

Figure 5. XR-MT images of the ABS_{post}/GO nanocomposites and their respective volume and surface area histograms.

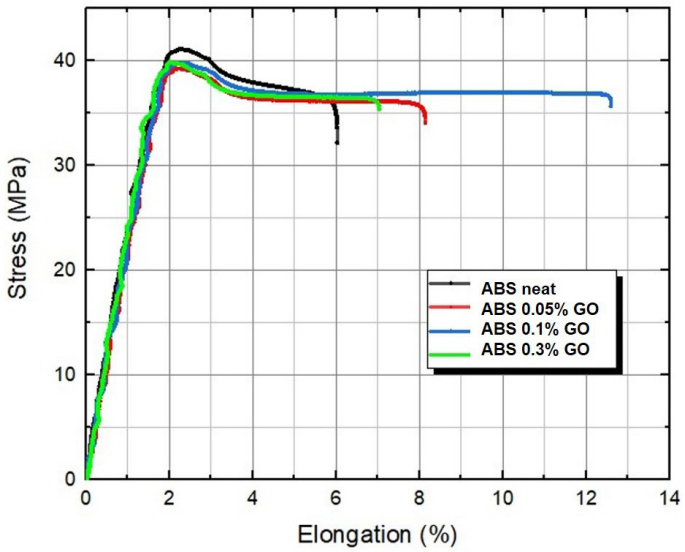

Figure 6. Stress-strain curves for ABS_{post} and ABS/GO nanocomposites.

Table 2. Mechanical properties of ABS_{post} and ABS_{post}/GO nanocomposites.

Sample	Young's Modulus (GPa)	Yield Strength (MPa)	Tensile at Break (MPa)	Elongation at Break (%)	Toughness (kJ/mm^3)
ABS_{post}	1.7 ± 0.3	44.0 ± 0.5	30.0 ± 2.6	5.6 ± 1.2	180.2 ± 40.7
ABS_{post}/GO 0.05	2.3 ± 0.5	38.3 ± 0.5	32.5 ± 0.8	9.1 ± 1.0	297.1 ± 36.2
ABS_{post}/GO 0.1	2.5 ± 0.1	39.6 ± 0.2	34.7 ± 0.9	11.9 ± 1.7	407.7 ± 63.1
ABS_{post}/GO 0.3	2.1 ± 0.4	39.8 ± 0.2	33.5 ± 2.3	8.2 ± 1.4	275.2 ± 52.5

present results close to low values of the range found in the literature. The polymer processing undergone by the ABS resin in the company probably did not lead to a significant degradation process.

Using a nanofiller may improve some of the ABSpost's mechanical properties in this context. However, results showed no significant variation in Young's modulus with GO incorporation. In fact, it was expected that Young´s Modulus would increase with the GO content, as can be calculated using the modified rule mixing equation[33]. A possible explanation is GO multilayers and agglomerates that could induce the superlubricity phenomenon[34], decreasing the value of Young´s modulus.

However, yield strength tends to decrease with the increasing amount of GO, from 44 MPa in ABSpost to approximately 39 MPa in all nanocomposites. One hypothesis that sustains this change is the superlubricity phenomenon that could occur between the GO layers and the polymer chains, where the nanolayers act as lubricants "sliding" between themselves, decreasing the tensile strength and increasing the elongation of the nanocomposites[35].

The tensile and elongation at break values also tend to increase until the 0.1% GO composition, which led to a rise in the toughness of ~ 125% for this composition compared to the ABSpost. This indicates excellent interfacial adhesion between filler and matrix and bonding between the functional groups of GO and the polymer[36]. A nanofiller aggregation may occur at 0.3% of the GO amount, as shown in the XR-MT analysis, thus decreasing the mechanical properties.

Figure 7 shows the impact strength of the ABS_{post} and the ABS_{post}/GO nanocomposites. ABS is known for its high impact resistance, which depends on the polybutadiene phase (PB) percentage on the terpolymer; this monomer contributes to the toughness and impact resistance[37]. Generally, the neat ABS resin presents high impact strength, around 260 J/m[38,39], or 25 kJ/m^2[40]. Here, it was used a post-industrial recycled ABS (ABS_{post}), which may have arisen from the waste of electronic products, which may contain many impurities and traces of other materials; besides that, the material already passed a cycle of processing parameters, which may have lost some properties due to thermal degradation[32]. So, the impact strength value for ABS_{post} was around 18 J/m. The necessary energy to break the specimen slightly increased as the amount of GO increased until 0.1 wt.% of the filler, reaching 20 J/m, indicating very well-dispersed fillers; consequently, the stress distribution occurred more uniformly. Figure 8 shows a surface fracture image of the ABS_{post}/GO 0.1 nanocomposite impact sample. As can be seen, the GO particle is very well attached to the ABS matrix, confirming the supposition made. Another exciting factor is that the thin sheet of GO shape can limit the development of cracks in the matrix in the V-notched specimen[41]. Further increasing

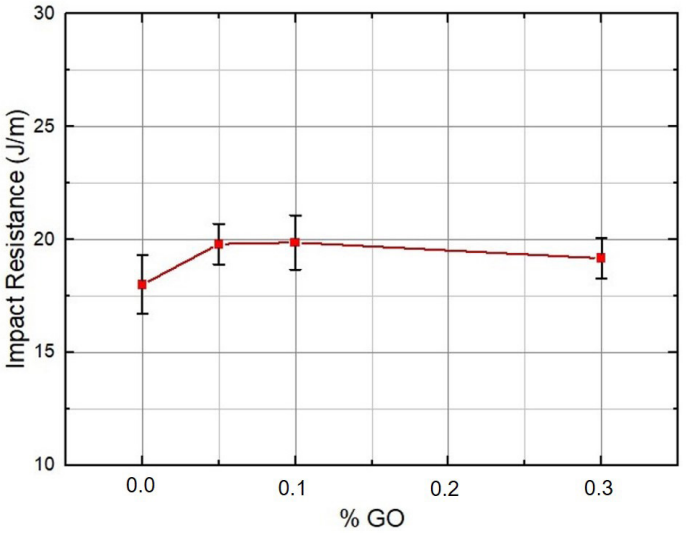

Figure 7. Impact Resistance of ABS_{post} and ABS_{post}/GO nanocomposites.

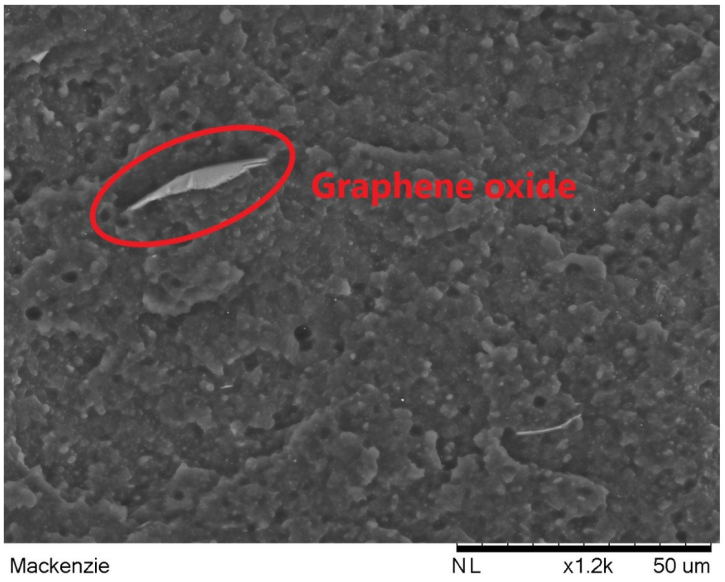

Figure 8. SEM image of the surface fracture of the ABS_{post}/GO 0.1 nanocomposite impact sample.

the filler content to 0.3 wt.%, the impact strength decreased probably at this higher concentration, it is more difficult to disperse the filler, and the formation of agglomerates occurs, as shown in XR-MT, causing stress concentrations areas, which reduces the impact strength. The nanocomposite gets brittle as the percentage of GO increases, and the reduction in the impact strength of polymers with the addition of GO was also reported in another research[42,43].

3.2.3 Dynamic mechanical analysis

Figure 9 shows the DMA results of ABS_{post} and the ABS_{post}/GO nanocomposites. From DMA, it was possible to obtain parameters such as storage modulus (E'), loss modulus (E"), and tan delta. E' decreases for all samples as the temperature increases due to a decreased stiffness resulting from increased mobility chains. Adding 0.05 or 0.1 wt.% of GO did not alter the E'. However, the composite with 0.3 wt.% of GO slightly increased the E' when compared with the other compositions in temperatures from approximately 60 to 100 °C, indicating that the energy absorbed by the material is higher, increasing stiffness and preventing chains from moving. Excess GO can maintain a plateau of E' for longer before reaching Tg. This was also verified for the composition with 0.1% GO but less intense. In other words, the formation of agglomerates (as seen in XR-MT images) hinders the mobility of the chains at higher temperatures. This mobility is only overcome when approaching Tg; all materials behave similarly.

The E" means the amount of energy the polymer dissipates, and for ABS_{post}/GO with 0.1 or 0.3 wt%. the E"

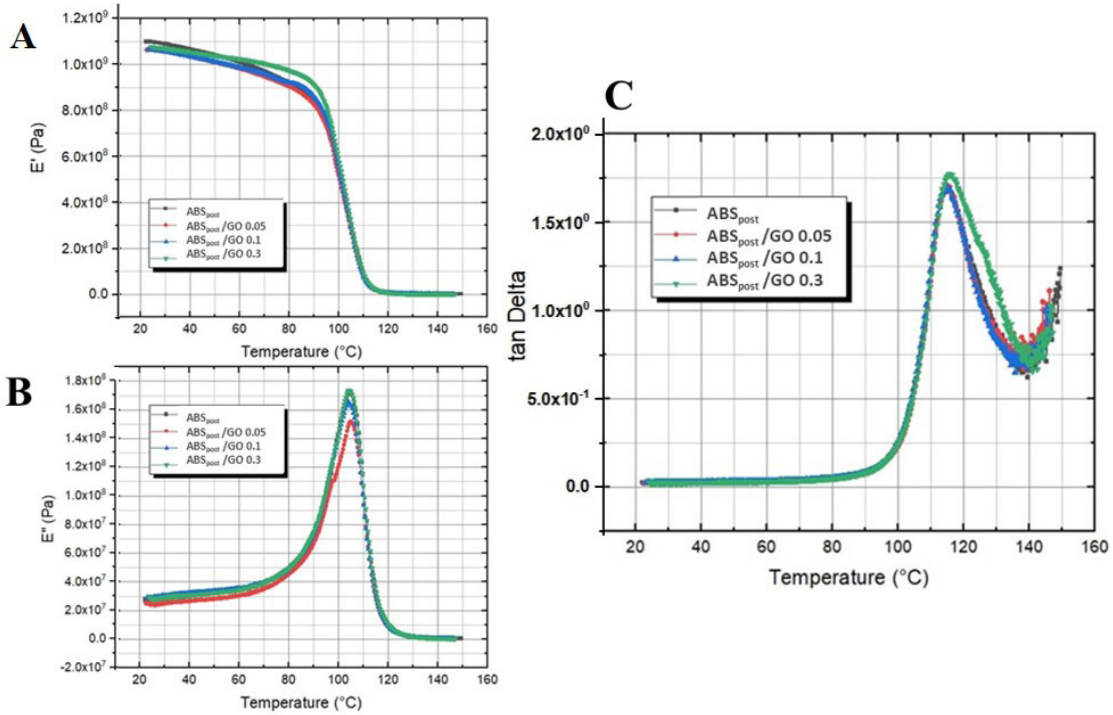

Figure 9. a) Elastic Modulus, b) Loss modulus, and c) Tan delta of ABS$_{post}$ and ABS$_{post}$/GO nanocomposites.

is similar to ABS. The E" of ABS$_{post}$/GO 0.05% slightly decreased compared to the ABS, indicating a decrease in energy dissipation. ABS$_{post}$/GO 0.05% presents a better filler dispersion level (as seen on XR-MT images), hindering the chain mobility and energy dissipation mechanism.

The tan delta (damping factor) is the relation between loss and storage modulus (tan delta = E"/E'), and the peak of tan delta in the graph, at approximately 115 °C, corresponds to the glass transition temperature (T_g) related to the SAN phase of ABS, where the material changes from rigid to elastic behavior, due to increase in mobility. The tan delta peak is the same for all compositions; the GO particles are probably not close to the SAN phase, or the filler content is not high enough to impact this polymer property. The GO incorporation does not show any variation in the tan delta peak height; only 0.3% of GO composition increases the damping factor of the ABS$_{post}$ matrix. The increase in the tan delta peak suggests that GO fortified the energy dissipation process. The presence of agglomerates in this composition (as seen on XR-MT images) leads to vacant spaces, and the chain polymer moves or rotates freely.

The coefficient of effectiveness, the C-factor, of the filler in the polymer matrix was calculated using the Equation 2:

$$C = \frac{E'g / E'r(composite)}{E'g / E'r(matrix)} \quad (2)$$

E'g and E'r are the values of E' in the glassy region (80°C) and the rubbery region (120°C), respectively. The effectiveness of the filler in the polymer decreases as the C value increases[44]. The values obtained for ABS$_{post}$/GO nanocomposites are shown in Table 3. The composite containing 0.1% of GO showed the lower value of the C parameter, indicating that the effectiveness of GO was maximum in ABS$_{post}$/GO 0.1, confirming again that this composition presents the best dispersion and polymer-particle largest contact area.

3.2.4 Rheological characterization

Figure 10 shows the viscosity as a function of the shear rate for steady-state measurements. It is possible to see that the filler has no significant influence on the matrix in the melted state since there is no substantial change in the shear viscosity behavior in the shear range studied. These results could indicate that the concentration used in this work does not influence the shear viscosity behavior at a steady state regime. This result suggests that the processability of the ABS/GO composite will not change compared to ABS without the filler.

Figure 11 shows the viscoelastic behavior of the polymer and the nanocomposites. In this work, it was possible to observe, within the displayed frequency range, that ABS$_{post}$ and nanocomposites with GO indicate that a plateau for the storage modulus (G') at low frequencies was approached, with G' > G", suggesting a nonterminal behavior. This elastic behavior for the ABS$_{post}$ can be attributed to the butadiene phase in the ABS$_{post}$ formulation[45,46]. The nonterminal behavior means that the long-range motion of the macromolecules is hindered, resulting in incomplete relaxation of polymer chains. At intermediate frequencies, G" is higher than G' due to the dissipative response observed due to the interplay of both phases, the butadiene phase and styrene-acrylonitrile phase, within the polymer structure. At higher frequencies

Table 3. C-factor obtained by DMA for ABS_{post} and ABS_{post}/GO nanocomposites.

Sample	E': glassy region 80°C (Pa)	E': rubbery region 120°C (Pa)	C-factor
ABS	9.22×10^8	7.24×10^6	-
ABS_{post}/GO 0.05	9.05×10^8	5.93×10^6	1.20
ABS_{post}/GO 0.1	9.21×10^8	6.33×10^6	1.14
ABS_{post}/GO 0.3	9.74×10^8	6.24×10^6	1.22

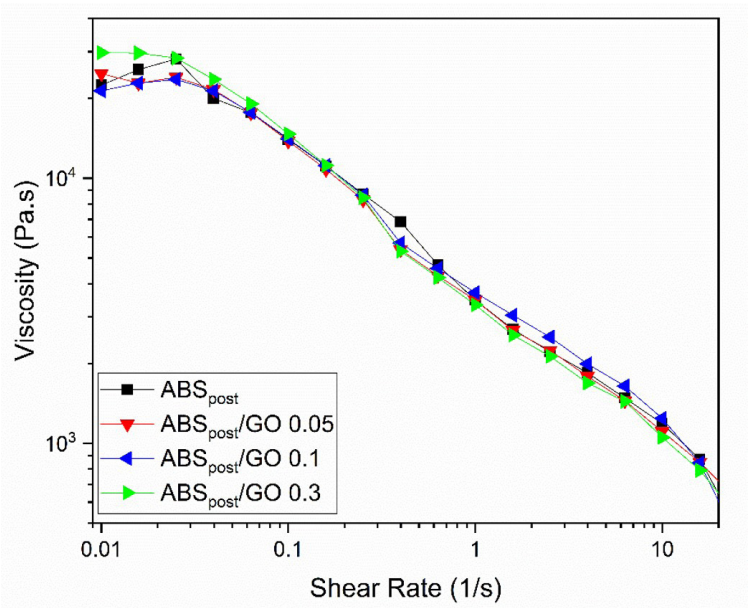

Figure 10. Viscosity as a function of shear rate of ABS_{post} and ABS_{post}/GO nanocomposites.

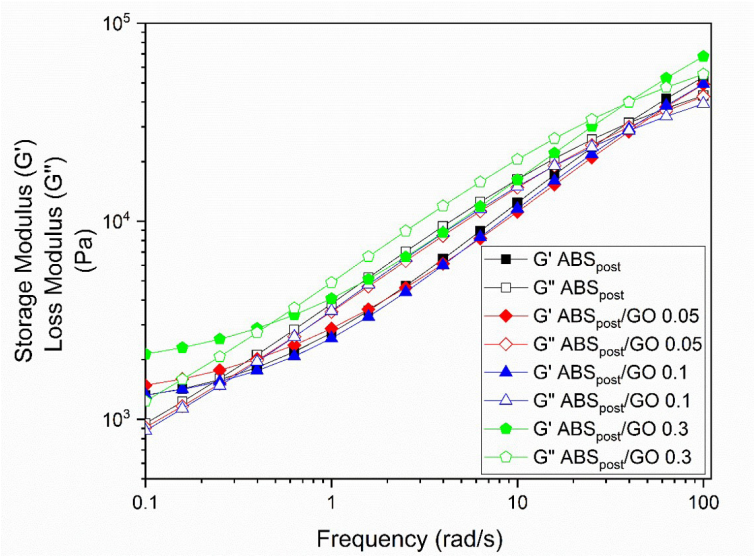

Figure 11. Storage and loss modulus of ABS_{post} and ABS_{post}/GO nanocomposites.

G' is higher than G'' again, indicating that the rubbery phase dominates the viscoelastic behavior at these frequencies[47]. Regarding the viscoelastic behavior of the nanocomposites, the materials follow the ABSpost matrix itself, mostly due to the low content of the filler, besides 0.3% of GO. Different behavior is observed at this concentration, with the G' and the G'' showing an enhancement, suggesting a mechanical reinforcement via modulus increase for the frequencies range analyzed. This result indicates that at a concentration of 0.3%, the GO can engage and interfere

in the polymer chain motion, as previously observed for dynamic mechanic analyses.

3.2.5 Thermal conductivity analysis

The thermal conductivity analysis was carried out to verify the influence of different amounts of GO on the thermal properties of ABS_{post}. The low thermal conductivity of polymers is a barrier that prevents their application in electronics due to their limited capability of spreading the heat. Adding a conductivity filler, such as graphene, to a thermally insulating matrix is a strategy to improve this property and is possibly applicable in the electronics and energy industry[48]. Nonetheless, some factors affect the thermal conductivity in polymer nanocomposites, including the properties of the graphene sheets, such as defect, lateral size, and surface chemistry; the dispersion/distribution of the filler within the matrix; and the filler content[49]. The GO has chemical functional groups, and the degree of oxidation can significantly affect the thermal conductivity of GO once the oxygen groups minimize the ability of phonon transport[50].

Phonons, like the heat conduction mechanism of crystalline materials, principally accomplish the thermal conductivity of graphene. The heat transfers from one layer of an atom to another in the form of vibrations, and due to the dense packing of atoms in the lattice and the strong chemical bonds between them, the heat transfer propagates as a wave and occurs rapidly. On the other hand, the heat transfer in the polymer is relatively more complicated and depends on various factors, such as the crystallinity and orientation of the chain. Still, it is known that the diffusion occurs slowly and causes disordered vibrations and rotation of the atoms, which reduces the thermal conductivity of the polymer. Considering the graphene polymer nanocomposites, the graphene creates interfaces within the matrix due to the large specific area, which will lead to phonon scattering and introduce high thermal resistance[51].

Figure 12 shows the thermal conductivity values of the ABS_{post} and ABS_{post}/GO systems with GO at four different temperatures (25, 40, 60, and 80°C). The thermal conductivity of ABS_{post} is very low, around 0.16 W/m.K at room temperature, and it increases as the temperature rises, reaching 0.27 W/m.K at 60 °C, and at 80°C, it turns to decrease. The temperature is very significant in the thermal conductivity of the nanocomposites. With the increase in the temperature (T > 300 K), the thermal conductivity of the monolayer graphene decreases because of the Umklapp scattering, and the interfacial thermal conductivity between GO and the polymer moderately increases, resulting from the weakening of the interfacial thermal barrier for heat transport[52].

The addition of GO in any filler content studied did not affect the thermal conductivity of ABS at 25 °C or 40 °C. However, in higher test temperatures (60°C and 80°C), it is possible to observe some changes: for the compositions with 0.1 and 0.3 wt.%, the thermal conductivity was 0.35 w/m.K, an increase of 30%, compared to ABS_{post} at the same temperature. This happens since GO tends to form a thermal conductivity network inside the polymer matrix and acts as a thermal conductivity channel. If the amount of graphene is below the percolation threshold, the fillers do not connect one to another and do not create a thermal conduction pathway. On the other hand, above the percolation threshold, heat transfer can occur through the thermal conduction pathway[51]. Another important observation is that Tg strongly influences polymer thermal conductivity variations. The decrease in the phonon velocity close to or above Tg is easily noticeable. So, the tendency for thermal conductivity to increase is stopped by the approach of the glass transition temperature[53].

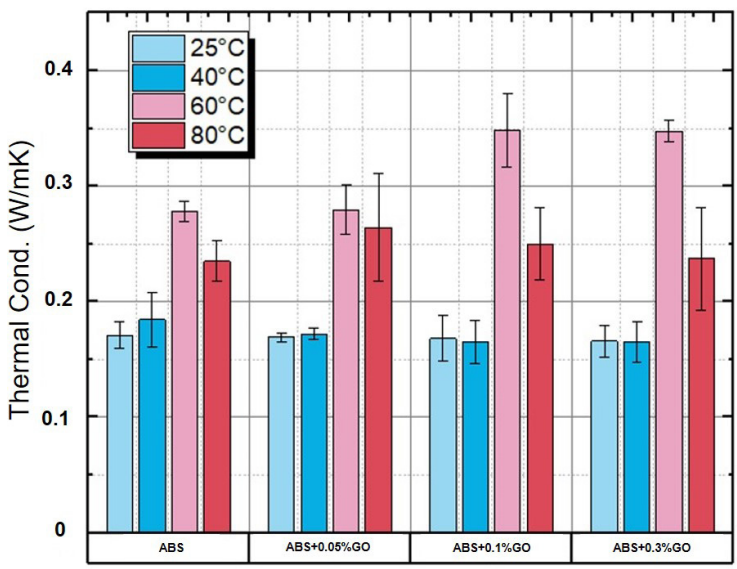

Figure 12. Thermal conductivity of ABS_{post} and ABS_{post}/GO nanocomposites in different temperatures.

4. Conclusion

It was investigated the effect of the addition of GO on the properties of post-consumer ABS, aiming to apply this polymer back to the consumer, minimizing the impact of wrong disposal and pollution on the environment. The thermal conductivity increased by 30% with the addition of 0.1 and 0.3 wt% of GO compared to the ABSpost; efficient heat management is crucial to dissipate excessive heat, improving the efficiency of electronic devices; with the increase in thermal conductivity; these materials are attractive for applications involving electronic circuit parts where heat dissipation is required. The mechanical properties of ABSpost also improved with the insertion of a small concentration of GO, as well as the toughness and impact strength. The XR-MT showed the best distribution and dispersion of the nanocomposites' fillers with smaller amounts of GO, corroborating the results of mechanical properties.

In short, this paper contributes to developing a new material that recovers the properties of post-consumer ABS from electronic product waste, a strategy to reduce pollution and be environmentally friendly.

5. Author's Contribution

- **Conceptualization –** Lucas Pacanaro de Lima; Natália Ferreira Braga.
- **Data curation –** Lucas Pacanaro de Lima; André Petraconi.
- **Formal analysis –** Lucas Pacanaro de Lima; Natália Ferreira Braga; André Petraconi.
- **Funding acquisition –** Guilhermino José Macêdo Fechine.
- **Investigation –** Lucas Pacanaro de Lima; André Petraconi.
- **Methodology –** Lucas Pacanaro de Lima; André Petraconi.
- **Project administration –** Guilhermino José Macêdo Fechine.
- **Resources –** Lidiane Cristina Costa; Ricardo Jorge Espanhol Andrade; Guilhermino José Macêdo Fechine.
- **Software –** NA.
- **Supervision –** Guilhermino José Macêdo Fechine.
- **Validation –** Lidiane Cristina Costa; Ricardo Jorge Espanhol Andrade; Guilhermino José Macêdo Fechine.
- **Visualization –** Natália Ferreira Braga; Lidiane Cristina Costa; Ricardo Jorge Espanhol Andrade; Guilhermino José Macêdo Fechine.
- **Writing – original draft –** Lucas Pacanaro de Lima; Natália Ferreira Braga.
- **Writing – review & editing –** Lidiane Cristina Costa; Ricardo Jorge Espanhol Andrade; Guilhermino José Macêdo Fechine.

6. Acknowledgements

The authors would like to acknowledge FAPESP – Fundação de Amparo à Pesquisa do Estado de São Paulo (2020/14302-2 and 2019/06620-7). The support provided by Conselho Nacional de Desenvolvimento Científico e Tecnológico (CNPq, Project Number: 305109/2022-7), CNPq National Institute of Science and Technology of Carbon Nanomaterials (INCT-Nanocarbono), CNPq National Institute of Science and Technology for Rheology of Complex Materials Applied to Advanced Technologies (INCT-Rhe9) grant 406765/2022-7. We also acknowledge the Rigaku for the X-ray Microtomography analysis.

7. References

1. Oliveira, I. M., Gimenez, J. C. F., Xavier, G. T. M., Ferreira, M. A. B., Silva, C. M. P., Camargo, E. R., & Cruz, S. A. (2024). Recycling ABS from WEEE with peroxo-modified surface of titanium dioxide particles: alteration on antistatic and degradation properties. *Journal of Polymers and the Environment*, *32*(3), 1122-1134. http://doi.org/10.1007/s10924-023-03021-7.
2. Vazquez, Y. V., & Barbosa, S. E. (2017). Process window for direct recycling of acrylonitrile-butadiene-styrene and high-impact polystyrene from electrical and electronic equipment waste. *Waste Management (New York, N.Y.)*, *59*, 403-408. http://doi.org/10.1016/j.wasman.2016.10.021. PMid:27769650.
3. Scaffaro, R., Botta, L., & Di Benedetto, G. (2012). Physical properties of virgin-recycled ABS blends: effect of post-consumer content and of reprocessing cycles. *European Polymer Journal*, *48*(3), 637-648. http://doi.org/10.1016/j.eurpolymj.2011.12.018.
4. Saxena, D., & Maiti, P. (2021). Utilization of ABS from plastic waste through single-step reactive extrusion of LDPE/ABS blends of improved properties. *Polymer*, *221*, 123626. http://doi.org/10.1016/j.polymer.2021.123626.
5. Brennan, L. B., Isaac, D. H., & Arnold, J. C. (2002). Recycling of acrylonitrile-butadiene-styrene and high-impact polystyrene from waste computer equipment. *Journal of Applied Polymer Science*, *86*(3), 572-578. http://doi.org/10.1002/app.10833.
6. Wang, J., Li, Y., Song, J., He, M., Song, J., & Xia, K. (2015). Recycling of acrylonitrile-butadiene-styrene (ABS) copolymers from waste electrical and electronic equipment (WEEE), through using an epoxy-based chain extender. *Polymer Degradation & Stability*, *112*, 167-174. http://doi.org/10.1016/j.polymdegradstab.2014.12.025.
7. Mao, N. D., Thanh, T. D., Thuong, N. T., Grillet, A.-C., Kim, N. H., & Lee, J. H. (2016). Enhanced mechanical and thermal properties of recycled ABS/nitrile rubber/nanofil N15 nanocomposites. *Composites. Part B, Engineering*, *93*, 280-288. http://doi.org/10.1016/j.compositesb.2016.03.039.
8. Lee, S. J., Yoon, S. J., & Jeon, I.-Y. (2022). Graphene/polymer nanocomposites: Preparation, mechanical properties, and application. *Polymers*, *14*(21), 4733. http://doi.org/10.3390/polym14214733. PMid:36365726.
9. Trivedi, D. N., & Rachchh, N. V. (2022). Graphene and its application in thermoplastic polymers as nano-filler: A review. *Polymer*, *240*, 124486. http://doi.org/10.1016/j.polymer.2021.124486.
10. Aumnate, C., Pongwisuthiruchte, A., Pattananuwat, P., & Potiyaraj, P. (2018). Fabrication of ABS/graphene oxide composite filament for fused filament fabrication (FFF) 3D printing. *Advances in Materials Science and Engineering*, *2830437*(1), 2830437. http://doi.org/10.1155/2018/2830437.
11. Dul, S., Fambri, L., & Pegoretti, A. (2016). Fused deposition modelling with ABS-graphene nanocomposites. *Composites. Part A, Applied Science and Manufacturing*, *85*, 181-191. http://doi.org/10.1016/j.compositesa.2016.03.013.

12. Waheed, Q., Khan, A. N., & Jan, R. (2016). Investigating the reinforcement effect of few layer graphene and multi-walled carbon nanotubes in acrylonitrile-butadiene-styrene. *Polymer*, *97*, 496-503. http://doi.org/10.1016/j.polymer.2016.05.070.
13. Lee, S. J., Baek, J., & Jeon, I.-Y. (2024). Preparation and characteristics of decene-functionalized graphitic nanoplatelets/acrylonitrile butadiene styrene hybrid nanocomposites. *Polymer*, *294*, 126727. http://doi.org/10.1016/j.polymer.2024.126727.
14. Du, J., & Cheng, H.-M. (2012). The fabrication, properties, and uses of graphene/polymer composites. *Macromolecular Chemistry and Physics*, *213*(10-11), 1060-1077. http://doi.org/10.1002/macp.201200029.
15. Fu, X., Lin, J., Liang, Z., Yao, R., Wu, W., Fang, Z., Zou, W., Wu, Z., Ning, H., & Peng, J. (2023). Graphene oxide as a promising nanofiller for polymer composite. *Surfaces and Interfaces*, *37*, 102747. http://doi.org/10.1016/j.surfin.2023.102747.
16. Shah, R., Kausar, A., Muhammad, B., & Shah, S. (2015). Progression from graphene and graphene oxide to high performance polymer-based nanocomposite: a review. *Polymer-Plastics Technology and Engineering*, *54*(2), 173-183. http://doi.org/10.1080/03602559.2014.955202.
17. Pinto, G. M., Silva, G. C., & Fechine, G. J. M. (2020). Effect of exfoliation medium on the morphology of multi-layer graphene oxide and its importance for poly(ethylene terephthalate)-based nanocomposites. *Polymer Testing*, *90*, 106742. http://doi.org/10.1016/j.polymertesting.2020.106742.
18. Farivar, F., Lay Yap, P., Karunagaran, R. U., & Losic, D. (2021). Thermogravimetric analysis (TGA) of graphene materials: effect of particle size of graphene, graphene oxide and graphite on thermal parameters. *Journal of Carbon Research*, *7*(2), 41. http://doi.org/10.3390/c7020041.
19. Zhang, Z., Schniepp, H. C., & Adamson, D. H. (2019). Characterization of graphene oxide: variations in reported approaches. *Carbon*, *154*, 510-521. http://doi.org/10.1016/j.carbon.2019.07.103.
20. Vorrada, L., Krit, T., Passakorn, E., Wanchai, B., & Achanai, B. (2013). Preparation and characterization of reduced graphene oxide sheets via water-based exfoliation and reduction methods. *Advances in Materials Science and Engineering*, *2013*(1), 923403. http://doi.org/10.1155/2013/923403.
21. Stobinski, L., Lesiak, B., Malolepszy, A., Mazurkiewicz, M., Mierzwa, B., Zemek, J., Jiricek, P., & Bieloshapka, I. (2014). Graphene oxide and reduced graphene oxide studied by the XRD, TEM and electron spectroscopy methods. *Journal of Electron Spectroscopy and Related Phenomena*, *195*, 145-154. http://doi.org/10.1016/j.elspec.2014.07.003.
22. Kudin, K. N., Ozbas, B., Schniepp, H. C., Prud'homme, R. K., Aksay, I. A., & Car, R. (2008). Raman spectra of graphite oxide and functionalized graphene sheets. *Nano Letters*, *8*(1), 36-41. http://doi.org/10.1021/nl071822y. PMid:18154315.
23. Muzyka, R., Drewniak, S., Pustelny, T., Chrubasik, M., & Gryglewicz, G. (2018). Characterization of graphite oxide and reduced graphene oxide obtained from different graphite precursors and oxidized by different methods using Raman spectroscopy. *Materials (Basel)*, *11*(7), 1050. http://doi.org/10.3390/ma11071050. PMid:29933564.
24. Kaniyoor, A., & Ramaprabhu, S. (2012). A Raman spectroscopic investigation of graphite oxide derived graphene. *AIP Advances*, *2*(3), 032183. http://doi.org/10.1063/1.4756995.
25. Prolongo, S. G., Jiménez-Suárez, A., Moriche, R., & Ureña, A. (2014). Graphene nanoplatelets thickness and lateral size influence on the morphology and behavior of epoxy composites. *European Polymer Journal*, *53*, 292-301. http://doi.org/10.1016/j.eurpolymj.2014.01.019.
26. Kaczmarek, Ł., Warga, T., Makowicz, M., Kyzioł, K., Bucholc, B., & Majchrzycki, Ł. (2020). The influence of the size and oxidation degree of graphene flakes on the process of creating 3D structures during its cross-linking. *Materials (Basel)*, *13*(3), 681. http://doi.org/10.3390/ma13030681. PMid:32028708.
27. Ramaraj, B. (2006). Mechanical and thermal properties of ABS and leather waste composites. *Journal of Applied Polymer Science*, *101*(5), 3062-3066. http://doi.org/10.1002/app.24113.
28. Song, P., Cao, Z., Meng, Q., Fu, S., Fang, Z., Wu, Q., & Ye, J. (2012). Effect of lignin incorporation and reactive compatibilization on the morphological, rheological, and mechanical properties of ABS resin. *Journal of Macromolecular Science, Part B: Physics*, *51*(4), 720-735. http://doi.org/10.1080/00222348.2011.609794.
29. Abdelhaleem, A. M. M., Abdellah, M. Y., Fathi, H. I., & Dewidar, M. (2016). Mechanical properties of ABS embedded with basalt fiber fillers. *Journal for Manufacturing Science and Production*, *16*(2), 69-74. http://doi.org/10.1515/jmsp-2016-0006.
30. Khan, M. M. K., Liang, R. F., Gupta, R., & Agarwal, S. (2005). Rheological and mechanical properties of ABS/PC blends. *Korea-Australia Rheology Journal*, *17*(1), 1-7. Retrieved in 2024, July 31, from https://www.researchgate.net/publication/268432181
31. Budin, S., Hyie, K. M., Yussof, H., Ishak, A., & Ginting, R. (2020). Investigation on mechanical properties of blend virgin and recycled acrylonitrile-butadiene-styrene (ABS) in injection molding. *Key Engineering Materials*, *833*, 8-12. http://doi.org/10.4028/www.scientific.net/KEM.833.8.
32. Teixeira, F. S. M., Peres, A. C. C., Gomes, T. S., Visconte, L. L. Y., & Pacheco, E. B. A. V. (2021). A review on the applicability of life cycle assessment to evaluate the technical and environmental properties of waste electrical and electronic equipment. *Journal of Polymer Environmental Science*, *29*(5), 1333-1349. http://doi.org/10.1007/s10924-020-01966-7.
33. Cremonezzi, J. M. O., Pinto, G. M., Mincheva, R., Andrade, R. J. E., Raquez, J.-M., & Fechine, G. J. M. (2023). The micromechanics of graphene oxide and molybdenum disulfide in thermoplastic nanocomposites and the impact to the polymer-filler interphase. *Composites Science and Technology*, *243*, 110236. http://doi.org/10.1016/j.compscitech.2023.110236.
34. Ferreira, E. H. C., Lima, L. P., & Fechine, G. J. M. (2020). The "superlubricity state" of carbonaceous fillers on polymer composites. *Macromolecular Chemistry and Physics*, *221*(16), 2000192. http://doi.org/10.1002/macp.202000192.
35. Ferreira, E. H. C., Andrade, R. J. E., & Fechine, G. J. M. (2019). The "superlubricity state" of carbonaceous fillers on polyethylene-based composites in a molten state. *Macromolecules*, *52*(24), 9620-9631. http://doi.org/10.1021/acs.macromol.9b01746.
36. Joynal Abedin, F. N., Hamid, H. A., Alkarkhi, A. F. M., Amr, S. S. A., Khalil, N. A., Ahmad Yahaya, A. N., Hossain, M. S., Hassan, A., & Zulkifli, M. (2021). The effect of graphene oxide and SEBS-g-MAH compatibilizer on mechanical and thermal properties of acrylonitrile-butadiene-styrene/talc composite. *Polymers*, *13*(18), 3180. http://doi.org/10.3390/polym13183180. PMid:34578081.
37. Campo, E. A. (2008). *Polymeric materials and properties.* In E. A. Campo (Ed.), *Selection of polymeric materials: How to select design properties from different standards* (pp. 1-39). USA: William Andrew. http://doi.org/10.1016/B978-081551551-7.50003-6.
38. Hwang, D., Lee, S. G., & Cho, D. (2021). Dual-sizing effects of carbon fiber on the thermal, mechanical, and impact properties of carbon fiber/ABS composites. *Polymers*, *13*(14), 2298. http://doi.org/10.3390/polym13142298. PMid:34301055.
39. Mazzucco, M. L. C., Marchesin, M. S., Fernandes, E. G., Costa, R. A., Marini, J., Bretas, R. E. S., & Bartoli, J. R. (2016). Nanocomposites of acrylonitrile-butadiene-styrene/

montmorillonite/styrene block copolymers: structural, rheological, mechanical and flammability studies on the effect of organoclays and compatibilizers using statistically designed experiments. *Journal of Composite Materials*, *50*(6), 771-782. http://doi.org/10.1177/0021998315581509.

40. Braga, N. F., Passador, F. R., Saito, E., & Cristovan, F. H. (2019). Effect of graphite content on the mechanical properties of acrylonitrile-butadiene-styrene (ABS). *Macromolecular Symposia*, *383*(1), 1800018. http://doi.org/10.1002/masy.201800018.
41. Liang, J.-Z. (2019). Impact fracture behavior and morphology of polypropylene/graphene nanoplatelets composites. *Polymer Composites*, *40*(S1), E511-E516. http://doi.org/10.1002/pc.24826.
42. Morales-Zamudio, L., Lozano, T., Caballero-Briones, F., Zamudio, M. A. M., Angeles-San Martin, M. E., de Lira-Gomez, P., Martinez-Colunga, G., Rodriguez-Gonzalez, F., Neira, G., & Sanchez-Valdes, S. (2021). Structure and mechanical properties of graphene oxide-reinforced polycarbonate. *Materials Chemistry and Physics*, *261*, 124180. http://doi.org/10.1016/j.matchemphys.2020.124180.
43. Sabet, M. (2023). The impact of graphene oxide on the mechanical and thermal strength properties of polycarbonate. *Journal of Elastomers and Plastics*, *55*(4), 511-525. http://doi.org/10.1177/00952443231160236.
44. Jyoti, J., Singh, B. P., Arya, A. K., & Dhakate, S. R. (2016). Dynamic mechanical properties of multiwall carbon nanotube reinforced ABS composites and their correlation with entanglement density, adhesion, reinforcement and C factor. *RSC Advances*, *6*(5), 3997-4006. http://doi.org/10.1039/C5RA25561A.
45. Münstedt, H. (1981). Rheology of rubber-modified polymer melts. *Polymer Engineering and Science*, *21*(5), 259-270. http://doi.org/10.1002/pen.760210503.
46. Sanchez, L. C., Beatrice, C. A. G., Lotti, C., Marini, J., Bettini, S. H. P., & Costa, L. C. (2019). Rheological approach for an additive manufacturing printer based on material extrusion. *International Journal of Advanced Manufacturing Technology*, *105*(5), 2403-2414. http://doi.org/10.1007/s00170-019-04376-9.
47. Münstedt, H. (2021). Rheological measurements and structural analysis of polymeric materials. *Polymers*, *13*(7), 1123. http://doi.org/10.3390/polym13071123. PMid:33915989.
48. Huang, C., Qian, X., & Yang, R. (2018). Thermal conductivity of polymers and polymer nanocomposites. *Materials Science and Engineering R Reports*, *132*, 1-22. http://doi.org/10.1016/j.mser.2018.06.002.
49. Zhao, H.-Y., Yu, M.-Y., Liu, J., Li, X., Min, P., & Yu, Z.-Z. (2022). Efficient preconstruction of three-dimensional graphene networks for thermally conductive polymer composites. *Nanomicro Letters*, *14*, 129. http://doi.org/10.1007/s40820-022-00878-6.
50. Chen, J., & Li, L. (2020). Effect of oxidation degree on the thermal properties of graphene oxide. *Journal of Materials Research and Technology*, *9*(6), 13740-13748. http://doi.org/10.1016/j.jmrt.2020.09.092.
51. Li, A., Zhang, C., & Zhang, Y.-F. (2017). Thermal conductivity of graphene-polymer composites: mechanisms, properties, and applications. *Polymers*, *9*(9), 437. http://doi.org/10.3390/polym9090437. PMid:30965752.
52. Wang, J., Li, C., Li, J., Weng, G. J., & Su, Y. (2021). A multiscale study of the filler-size and temperature dependence of the thermal conductivity of graphene-polymer nanocomposites. *Carbon*, *175*, 259-270. http://doi.org/10.1016/j.carbon.2020.12.086.
53. Santos, W. N., Sousa, J. A., & Gregorio, R., Jr. (2013). Thermal conductivity behaviour of polymers around glass transition and crystalline melting temperatures. *Polymer Testing*, *32*(5), 987-994. http://doi.org/10.1016/j.polymertesting.2013.05.007.

Received: July 31, 2024
Revised: Nov. 20, 2024
Accepted: Jan. 07, 2025